

Free vibration analysis of thick CGFR annular sector plates resting on elastic foundations

Vahid Tahouneh*

Department of Mechanical Engineering, Islamshahr Branch, Islamic Azad University, Tehran, Iran

(Received April 7, 2013, Revised March 25, 2014, Accepted April 4, 2014)

Abstract. This paper deals with free vibration analysis of continuous grading fiber reinforced (CGFR) and bi-directional FG annular sector plates on two-parameter elastic foundations under various boundary conditions, based on the three-dimensional theory of elasticity. The plates with simply supported radial edges and arbitrary boundary conditions on their circular edges are considered. A semi-analytical approach composed of differential quadrature method (DQM) and series solution is adopted to solve the equations of motion. Some new results for the natural frequencies of the plate are prepared, which include the effects of elastic coefficients of foundation, boundary conditions, material and geometrical parameters. Results indicate that the non-dimensional natural frequency parameter of a functionally graded fiber volume fraction is larger than that of a discrete laminated and close to that of a 2-layer. It results that the CGFR plate attains natural frequency higher than those of traditional discretely laminated composite ones and this can be a benefit when higher stiffness of the plate is the goal and that is due to the reduction in spatial mismatch of material properties. Moreover, it is shown that a graded ceramic volume fraction in two directions has a higher capability to reduce the natural frequency than conventional one-dimensional functionally graded material. The multidirectional graded material can likely be designed according to the actual requirement and it is a potential alternative to the unidirectional functionally graded material. The new results can be used as benchmark solutions for future researches.

Keywords: free vibration; continuous grading fiber reinforcement; bi-directional FG plates; thick annular sector plates; pasternak elastic foundations; three-dimensional elasticity

1. Introduction

New class of materials known as “functionally graded materials” (FGMs) has attracted much attention as advanced structural materials in many structural members used in situations where large temperature gradients are encountered. FGMs are designed so that material properties vary smoothly and continuously through the thickness from the surface of a ceramic exposed to high temperature to that of a metal on the other surface. The mechanical properties are graded in the thickness direction according to volume fraction power-law distribution.

Most of the previous studies on the free vibration of plates are based on the two-dimensional theories, such as the classical plate theory, the first- and the higher- order shear deformation plate

*Corresponding author, Ph.D. Candidate, E-mail: vahid.th1982@gmail.com, v.tahouneh@iausr.ac.ir

theories. These plate theories neglect transverse normal deformations, and generally assume that a plane stress state of deformation prevails in the plate. These assumptions may be appropriate for thin plates. Ramakris and Kunukkas (1973) provided a closed-form analytical solution for free vibration of an annular sector plate with radial edges simply supported. Mukhopadhyay (1979, 1982) used a semi-analytical method and Srinivasan and Thiruvengkatachari (1983, 1986) used the integral equation technique to analyze the vibrations of annular sector plates, respectively. Kim and Dickinson (1989) used one-dimensional (1-D) orthogonal polynomials and Liew and Lam (1993) used two-dimensional (2-D) orthogonal polynomials as admissible functions to study the free vibration of annular sector plates by the Rayleigh-Ritz method. McGee *et al.* (1995) considered the effect of stress singularities on the vibration analysis of thick annular sector plates and presented the corner functions to improve the convergence of the numerical solutions.

The vibration analyses of FG plates on elastic foundations are mostly limited and were performed based on the two-dimensional theories, such as the classical plate theory, the first- and the higher-order shear deformation plate theories (Yang and Shen 2001, Cheng and Kitipornchai 1999, Cheng and Batra 2000, Yang and Shen 2003, Hosseini-Hashemi *et al.* 2010a, b). However, a few papers have been found in the literature about the vibrations of annular sector plates based on the three-dimensional (3-D) elasticity theory. Houmat (2004) used the hierarchical finite element method and Liew *et al.* (2001) used the 2-D orthogonal polynomials in the Ritz method to analyze the free vibration of thick annular sector plates, Zhou *et al.* (2009) used the Chebyshev-Ritz method to study the free vibration of thick annular sector plates, Nie and Zhong (2008) investigated the free and forced vibration analysis of FGM annular sector plates with simply-supported radial edges by using a semi-analytical approach. Yas and Tahouneh (2012) investigated the free vibration analysis of thick FG annular plates on Pasternak elastic foundations based on the three-dimensional elasticity theory.

Zhou *et al.* (2004) studied free vibration characteristics of rectangular plates resting on elastic foundation based on the three-dimensional, linear and small strain elasticity theory. The Ritz method was used to derive the eigenvalue equation of the rectangular plate by augmenting the strain energy of the plate with the potential energy of the elastic foundation. Zhou *et al.* (2006) studied three-dimensional vibration characteristics of thick circular plates resting on an elastic foundation. The analysis was based on the three-dimensional theory of elasticity. Lü *et al.* (2008) used a semi-analytical elasticity solution for bending and thermal deformations of functionally graded beams with various end conditions, using the state space-based differential quadrature method. The beams are assumed to be macroscopically isotropic, with Young's modulus varying exponentially along the thickness and longitudinal directions, while Poisson's ratio remaining constant. Lü *et al.* (2009) used a three-dimensional elasticity solution based on differential quadrature method to investigate the displacement and stress fields of a multi-directional functionally graded plate. Nie and Zhong (2010) studied the free vibration of FG plates without elastic foundation using DQM. They assumed the material properties of the FG plate having an exponent-law variation along the thickness, radial direction or both directions. To the authors' best knowledge, researches on the vibration of thick continuous grading fiber reinforced (CGFR) and bi-directional FG annular sector plates on a two-parameter elastic foundation based on the three-dimensional theory of elasticity, have not been seen until now.

2. Problem description

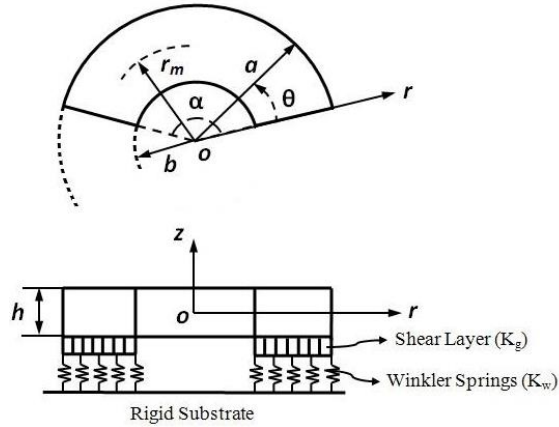


Fig. 1 Geometry and coordinate system of an annular sector plate resting on a two-parameter elastic foundation

Consider an annular sector plate resting on a two-parameter elastic foundation in a cylindrical coordinate system (r, θ, z) , as depicted in Fig. 1, where a, b, r_m and h are outer/inner radius, mean radius and thickness of the plate, respectively. The plate is supported by an elastic foundation with Winkler's (normal) and Pasternak's (shear) coefficients. It is assumed that the plate has been continuously graded in the thickness and radial directions.

3. Estimation of effective material properties

The effective mechanical properties of the continuous fiber reinforced plate are obtained based on a micromechanical model as follows (Shen 2009, Valery and Vasiliev 2001)

$$E_1 = V_f E_1^f + V_m E_1^m \tag{1}$$

$$\frac{1}{E_i} = \frac{V_f}{E_i^f} + \frac{V_m}{E_i^m} - V_f V_m \frac{\nu_f^2 E_i^m / E_i^f + \nu_m^2 E_i^f / E_i^m - 2\nu^f \nu^m}{V_f E_i^f + V_m E_i^m} \tag{2}$$

($i = 2 \text{ and } 3$)

$$\frac{1}{G_{ij}} = \frac{V_f}{G_{ij}^f} + \frac{V_m}{G_{ij}^m} \quad (ij = 12, 13 \text{ and } 23) \tag{3}$$

$$\nu_{ij} = V_f \nu^f + V_m \nu^m \quad (ij = 12, 13 \text{ and } 23) \tag{4}$$

$$\rho = V_f \rho^f + V_m \rho^m \tag{5}$$

Where $E_{ij}, G_{ij}, \nu_{ij}, \rho, V_f$ and V_m are elasticity modulus, shear modulus, Poisson's ratio, density, fiber

volume and matrix volume fractions, respectively. For orthotropic plate, we assume the following specific power-law variation of the reinforcement volume fraction (Jacob and Senthil 2006)

$$V_m = V_i + (V_o - V_i)\left(\frac{z}{h} + 0.5\right)^p \quad (6)$$

Where V_i and V_o which have values that range from 0 to 1, denote the volume fractions (matrix or fiber) on the lower and upper surfaces, respectively. The exponent “ P ” controls the volume fraction profile in the thickness direction of the plate. The volume fraction profile through the thickness (z/h) is illustrated in Fig. 2. In this figure it is assumed the matrix volume fractions for a CGFR annular plate with graded fiber volume fraction are $V_i=1$ (100 % matrix constituent) and $V_o=0.25$ (25 % matrix constituent) on the lower and upper surfaces, respectively. In this figure the matrix volume fraction decreases from 1 at $z/h = -0.5$ to 0.25 at $z/h = 0.5$. At z/h away from 0.5, the rate of increase of the matrix volume fraction for $p < 1$ is high compared to $p > 1$ and at z/h closer to 0.5, the rate of increase of the matrix volume fraction for $p > 1$ is much higher than for $p < 1$.

In order to investigate 3D dynamic response of thick bi-directional FG annular sector plates resting on a two-parameter elastic foundation, it is considered that the fiber volume fraction follows a 2-D six-parameter power-law distribution as follows

$$V_f = \left[\left(\frac{1}{2} - \frac{r-r_m}{a-b} \right) + \alpha_r \left(\frac{1}{2} + \frac{r-r_m}{a-b} \right)^{\beta_r} \right]^{\gamma_r} (V_b - V_a) + V_a \left[\alpha_z \left(\frac{1}{2} + \frac{z}{h} \right)^{\beta_z} + 1 - \left(\frac{1}{2} + \frac{z}{h} \right)^{\gamma_z} \right] \quad (7)$$

Where the radial volume fraction index γ_r , and the parameters α_r , β_r and the thickness volume fraction index γ_z , and the parameters α_z , β_z govern the material variation profile through the radial and along the thickness directions, respectively. The volume fractions V_a and V_b , which have values that range from 0 to 1, denote the ceramic volume fractions of the two different isotropic materials. For example, with assumption $V_b=1$ and $V_a=0.3$, some material profiles through the radial ($\mu_r=(r-r_m)/(a-b)$) and thickness ($\mu_z=z/h$) directions are illustrated in Fig. 3. As can be seen from Fig. 3(a), the classical volume fraction profile through the radial and thickness directions is presented as a special case of the 2-D power-law distribution by setting $\gamma_r = \gamma_z = 4$, and $\alpha_r = \alpha_z = 0$. With another choice of the parameters α_r , β_r , α_z and β_z , it is possible to obtain symmetric and

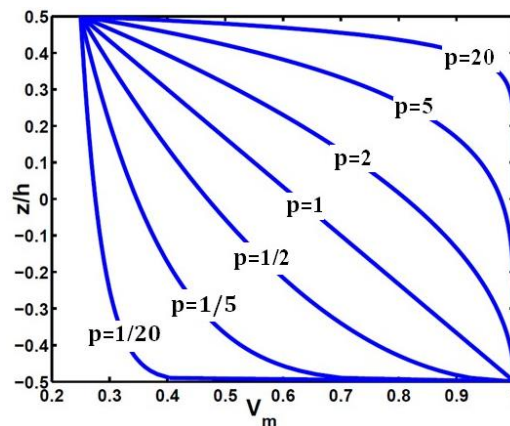


Fig. 2 Variations of the volume fraction of the matrix phase (V_m) through the thickness of the plate for different values of p

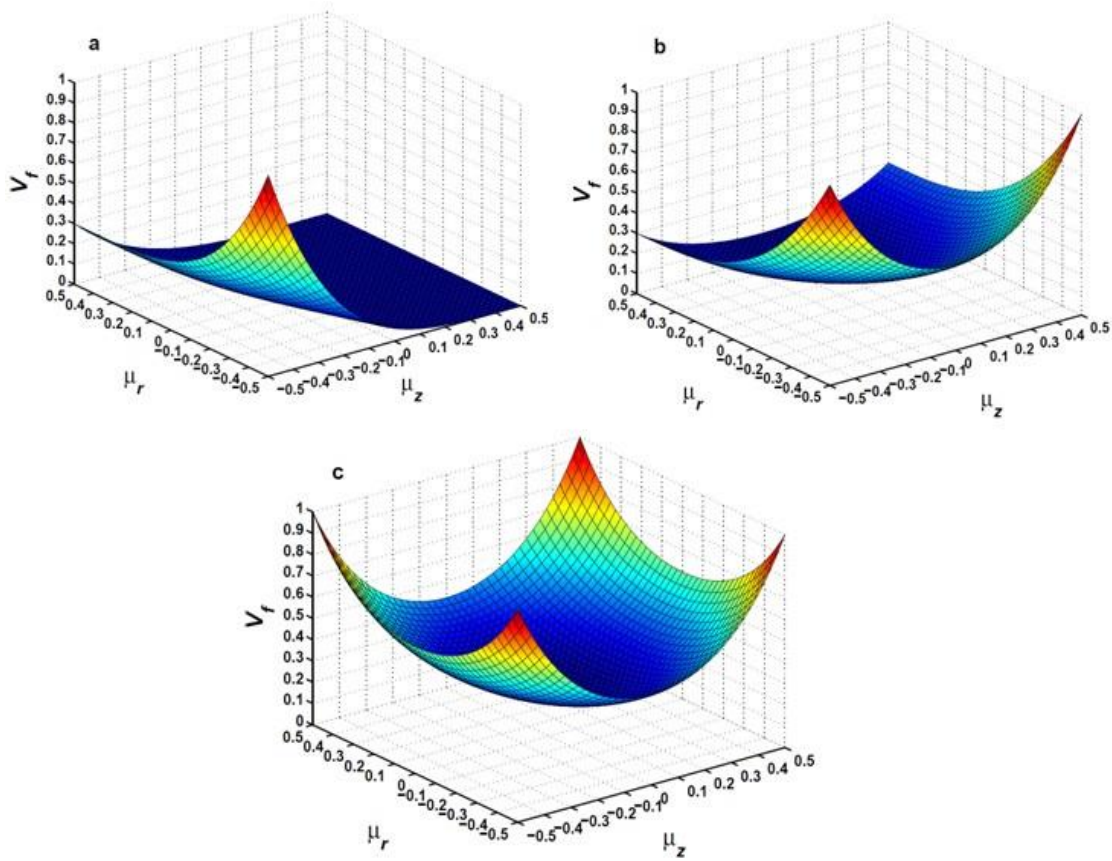


Fig. 3 The variations of the volume fraction profile in the radial and thickness directions of the plate (a) $\gamma_r = \gamma_z = 4$, $\alpha_r = \alpha_z = 0$, (b) $\gamma_r = \gamma_z = 3$, $\beta_r = 2$, $\alpha_r = 1$, $\alpha_z = 0$, (c) $\gamma_r = \gamma_z = 3$, $\beta_r = \beta_z = 2$, $\alpha_r = \alpha_z = 1$

classical volume fraction profiles through the thickness and radial directions, respectively as shown in Fig. 3(b). This Figure shows a classical profile versus μ_r and a symmetric profile versus μ_z . Fig. 3(c) illustrates symmetric profiles through the radial and thickness directions obtained by setting $\alpha_r = \alpha_z = 1$ and $\beta_r = \beta_z = 2$.

The effective material properties of the isotropic 2-D FGMs are determined in terms of the local volume fractions and material properties of the two isotropic phases by the Mori-Tanaka scheme. The Mori-Tanaka scheme (Mori and Tanaka 1973, Benveniste 1987) for estimating the effective moduli is applicable to regions of the graded microstructure that have a well-defined continuous matrix and a discontinuous particulate phase. It takes into account the interaction of the elastic fields among neighboring inclusions. It is assumed that the matrix phase, denoted by the subscript m , is reinforced by spherical particles of a particulate phase, denoted by the subscript c . In this notation, K_m and G_m are the bulk modulus and the shear modulus, respectively, and V_m is the volume fraction of the matrix phase. K_c , G_c and V_c are the corresponding material properties and the volume fraction of the particulate phase. Note that $V_m + V_c = 1$, the Lamé constant λ is related to the bulk and the shear moduli by $\lambda = K - 2G/3$, and the stress-temperature modulus is related to the coefficient of thermal expansion by $\beta = (3\lambda + 2G)\alpha = 3K\alpha$. The following estimates for the effective

Table 1 Material properties of aluminum and silicon carbide

	Young's Modulus, E (Gpa)	Poisson's ratio, ν	Mass density, ρ (kg/m^3)
Al	70	0.30	2,707
Silicon carbide (SiC)	410	0.170	3,100

local bulk modulus K and shear modulus G are useful for a random distribution of isotropic particles in an isotropic matrix

$$\frac{K - K_m}{K_c - K_m} = \frac{V_c}{1 + (1 - V_c)(K_c - K_m)/(K_m + (4/3)K_m)} \quad (8)$$

$$\frac{G - G_m}{G_c - G_m} = \frac{V_c}{1 + (1 - V_c)(G_c - G_m)/(G_m + f_m)} \quad (9)$$

Where $f_m = G_m(9K_m + 8G_m)/6(K_m + 2G_m)$. The effective values of Young's modulus, E , and Poisson's ratio, ν , are found from

$$E = \frac{9KG}{3K + G}, \nu = \frac{3K - 2G}{2(3K + G)} \quad (10)$$

We choose a metal/ceramic annular sector plate with the metal (Al) taken as the matrix phase and the ceramic (SiC) taken as the particulate phase. The material properties of aluminum and silicon carbide are listed in Table 1 (Vel and Batra 2002 and Vel 2010).

4. Theoretical formulations

Without consideration of body forces, the equations of motion are

$$\begin{aligned} \frac{\partial \sigma_r}{\partial r} + \frac{1}{r} \frac{\partial \tau_{r\theta}}{\partial \theta} + \frac{\partial \tau_{rz}}{\partial z} + \frac{\sigma_r - \sigma_\theta}{r} &= \rho \frac{\partial^2 u_r}{\partial t^2} \\ \frac{\partial \tau_{r\theta}}{\partial r} + \frac{1}{r} \frac{\partial \sigma_\theta}{\partial \theta} + \frac{\partial \tau_{\theta z}}{\partial z} + \frac{2\tau_{r\theta}}{r} &= \rho \frac{\partial^2 u_\theta}{\partial t^2} \\ \frac{\partial \tau_{rz}}{\partial r} + \frac{1}{r} \frac{\partial \tau_{\theta z}}{\partial \theta} + \frac{\partial \sigma_z}{\partial z} + \frac{\tau_{rz}}{r} &= \rho \frac{\partial^2 u_z}{\partial t^2} \end{aligned} \quad (11)$$

σ_r , σ_θ and σ_z are axial stress components, and $\tau_{r\theta}$, $\tau_{\theta z}$ and τ_{rz} are shear stress components, u_r , u_θ and u_z are displacement components, ρ denotes material density, and t is time. The relations between the strain and the displacement are

$$\begin{aligned} \varepsilon_r &= \frac{\partial u_r}{\partial r}, \varepsilon_\theta = \frac{u_r}{r} + \frac{1}{r} \frac{\partial u_\theta}{\partial \theta}, \varepsilon_z = \frac{\partial u_z}{\partial z}, \\ \gamma_{\theta z} &= \frac{\partial u_\theta}{\partial z} + \frac{1}{r} \frac{\partial u_z}{\partial \theta}, \gamma_{rz} = \frac{\partial u_r}{\partial z} + \frac{\partial u_z}{\partial r}, \\ \gamma_{r\theta} &= \frac{1}{r} \frac{\partial u_r}{\partial \theta} + \frac{\partial u_\theta}{\partial r} - \frac{u_\theta}{r} \end{aligned} \quad (12)$$

where $\epsilon_r, \epsilon_\theta, \epsilon_z, \gamma_{\theta z}, \gamma_{r\theta}$ and γ_{rz} are strain components. The constitutive equations for orthotropic materials are

$$\begin{pmatrix} \sigma_r \\ \sigma_\theta \\ \sigma_z \\ \tau_{z\theta} \\ \tau_{rz} \\ \tau_{r\theta} \end{pmatrix} = \begin{bmatrix} c_{11} & c_{12} & c_{13} & 0 & 0 & 0 \\ c_{12} & c_{22} & c_{23} & 0 & 0 & 0 \\ c_{13} & c_{23} & c_{33} & 0 & 0 & 0 \\ 0 & 0 & 0 & c_{44} & 0 & 0 \\ 0 & 0 & 0 & 0 & c_{55} & 0 \\ 0 & 0 & 0 & 0 & 0 & c_{66} \end{bmatrix} \begin{pmatrix} \epsilon_r \\ \epsilon_\theta \\ \epsilon_z \\ \gamma_{z\theta} \\ \gamma_{rz} \\ \gamma_{r\theta} \end{pmatrix} \tag{13}$$

Where c_{ij} are material elastic stiffness coefficients.

Using the three-dimensional constitutive relations and the strain-displacement relations, the equations of motion in terms of displacement components for a linear elastic FG plate with infinitesimal deformations can be written as

$$\begin{aligned} & c_{11} \frac{\partial^2 u_r}{\partial r^2} + c_{12} \left(-\frac{1}{r^2} \frac{\partial u_\theta}{\partial \theta} + \frac{1}{r} \frac{\partial^2 u_\theta}{\partial r \partial \theta} + \frac{1}{r} \frac{\partial u_r}{\partial r} - \frac{1}{r^2} u_r \right) + c_{13} \frac{\partial^2 u_z}{\partial r \partial z} + \frac{\partial c_{11}}{\partial r} \frac{\partial u_r}{\partial r} \\ & + \frac{\partial c_{12}}{\partial r} \left(\frac{u_r}{r} + \frac{1}{r} \frac{\partial u_\theta}{\partial \theta} \right) + \frac{\partial c_{13}}{\partial r} \frac{\partial u_z}{\partial z} + \frac{c_{66}}{r} \left[\frac{\partial^2 u_\theta}{\partial \theta \partial r} + \frac{1}{r} \frac{\partial^2 u_r}{\partial \theta^2} - \frac{1}{r} \frac{\partial u_\theta}{\partial \theta} \right] + \frac{\partial c_{55}}{\partial z} \left(\frac{\partial u_r}{\partial z} + \frac{\partial u_z}{\partial r} \right) + \\ & c_{55} \left(\frac{\partial^2 u_r}{\partial z^2} + \frac{\partial^2 u_z}{\partial z \partial r} \right) + \frac{1}{r} \left[c_{11} \frac{\partial u_r}{\partial r} + c_{12} \left(\frac{u_r}{r} + \frac{1}{r} \frac{\partial u_\theta}{\partial \theta} \right) + c_{13} \frac{\partial u_z}{\partial z} - c_{12} \frac{\partial u_r}{\partial r} - c_{22} \left(\frac{u_r}{r} + \frac{1}{r} \frac{\partial u_\theta}{\partial \theta} \right) - \right. \\ & \left. c_{23} \frac{\partial u_z}{\partial z} \right] = \rho \frac{\partial^2 u_r}{\partial t^2} \end{aligned} \tag{14}$$

$$\begin{aligned} & c_{66} \left(\frac{-1}{r^2} \frac{\partial u_r}{\partial \theta} + \frac{1}{r} \frac{\partial^2 u_r}{\partial r \partial \theta} + \frac{\partial^2 u_\theta}{\partial r^2} + \frac{u_\theta}{r^2} - \frac{1}{r} \frac{\partial u_\theta}{\partial r} \right) + \frac{\partial c_{66}}{\partial r} \left(\frac{1}{r} \frac{\partial u_r}{\partial \theta} + \frac{\partial u_\theta}{\partial r} - \frac{u_\theta}{r} \right) + \\ & \frac{1}{r} \left(c_{12} \frac{\partial^2 u_r}{\partial \theta \partial r} + c_{22} \left(\frac{1}{r} \frac{\partial u_r}{\partial \theta} + \frac{1}{r} \frac{\partial^2 u_\theta}{\partial \theta^2} \right) + c_{23} \frac{\partial^2 u_z}{\partial \theta \partial z} \right) + c_{44} \left(\frac{\partial^2 u_\theta}{\partial z^2} + \frac{1}{r} \frac{\partial^2 u_z}{\partial z \partial \theta} \right) + \end{aligned} \tag{15}$$

$$\begin{aligned} & \frac{\partial c_{44}}{\partial z} \left(\frac{\partial u_\theta}{\partial z} + \frac{1}{r} \frac{\partial u_z}{\partial \theta} \right) + \frac{2c_{66}}{r} \left(\frac{1}{r} \frac{\partial u_r}{\partial \theta} + \frac{\partial u_\theta}{\partial r} - \frac{u_\theta}{r} \right) = \rho \frac{\partial^2 u_\theta}{\partial t^2} \\ & c_{55} \left(\frac{\partial^2 u_r}{\partial r \partial z} + \frac{\partial^2 u_z}{\partial r^2} \right) + \frac{\partial c_{55}}{\partial r} \left(\frac{\partial u_r}{\partial z} + \frac{\partial u_z}{\partial r} \right) + \frac{c_{44}}{r} \left(\frac{\partial^2 u_\theta}{\partial \theta \partial z} + \frac{1}{r} \frac{\partial^2 u_z}{\partial \theta^2} \right) + c_{13} \frac{\partial^2 u_r}{\partial z \partial r} + \\ & c_{23} \left(\frac{1}{r} \frac{\partial u_r}{\partial z} + \frac{1}{r} \frac{\partial^2 u_\theta}{\partial \theta \partial z} \right) + c_{33} \frac{\partial^2 u_z}{\partial z^2} + \frac{\partial c_{13}}{\partial z} \frac{\partial u_r}{\partial r} + \frac{\partial c_{23}}{\partial z} \left(\frac{u_r}{r} + \frac{1}{r} \frac{\partial u_\theta}{\partial \theta} \right) + \frac{\partial c_{33}}{\partial z} \frac{\partial u_z}{\partial z} + \end{aligned} \tag{16}$$

$$\frac{c_{55}}{r} \left(\frac{\partial u_r}{\partial z} + \frac{\partial u_z}{\partial r} \right) = \rho \frac{\partial^2 u_z}{\partial t^2}$$

Eqs. (14)-(15) represent the in-plane equations of motion along the r and θ -axes, respectively; and Eq. (16) is the transverse or out-of-plane equation of motion. The related boundary conditions are as follows at $z = -h/2$

$$\begin{aligned} \tau_{zr} &= 0, \\ \tau_{z\theta} &= 0, \\ \sigma_z &= K_w u_z - K_g \left(\frac{\partial^2 u_z}{\partial r^2} + \frac{1}{r} \frac{\partial u_z}{\partial r} + \frac{1}{r^2} \frac{\partial^2 u_z}{\partial \theta^2} \right) \end{aligned} \quad (17)$$

at $z = h/2$

$$\tau_{zr} = 0, \tau_{z\theta} = 0, \sigma_z = 0 \quad (18)$$

K_w and K_g are the Winkler and shearing layer elastic coefficients of the foundation.

In this paper three different kinds of boundary conditions are considered: Clamped-Clamped (C-C), Simply supported-Clamped (S-C) and Free-Clamped (F-C).

The boundary conditions at edges are

-Clamped ($r=b$)-Clamped ($r=a$):

$$\begin{aligned} \text{at } r=a & \quad u_r = u_\theta = u_z = 0 \\ \text{at } r=b & \quad u_r = u_\theta = u_z = 0 \end{aligned} \quad (19)$$

-Simply supported ($r=b$)-Clamped ($r=a$):

$$\begin{aligned} \text{at } r=b & \quad u_\theta = u_z = \sigma_r = 0 \\ \text{at } r=a & \quad u_r = u_\theta = u_z = 0 \end{aligned} \quad (20)$$

-Free ($r=b$)-Clamped ($r=a$):

$$\begin{aligned} \text{at } r=a & \quad u_r = u_\theta = u_z = 0 \\ \text{at } r=b & \quad \sigma_r = \tau_{r\theta} = \tau_{rz} = 0 \end{aligned} \quad (21)$$

5. Solution procedure

It is difficult to solve analytically the equations of motion, if it is not impossible. Hence, one should use an approximate method to find a solution. According to some recently studies (Hosseini-Hashemi *et al.* 2010, Nie and Zhong 2008, 2010, Tahouneh and yas 2012, 2013) differential quadrature method is a really powerful method for vibration analysis of plates. One can compare DQM solution procedure with the other two widely used traditional methods for plate analysis, i.e., Rayleigh-Ritz method and FEM. The main difference between the DQM and the other methods is how the governing equations are discretized. In DQM, the governing equations and boundary conditions are directly discretized, and thus elements of stiffness and mass matrices are evaluated directly. But in Rayleigh- Ritz and FEMs, the weak form of the governing equations should be developed and the boundary conditions are satisfied in the weak form. Generally by doing so larger number of integrals with increasing amount of differentiation should be done to arrive at the element matrices. In addition, the number of degrees of freedom will be increased for an acceptable accuracy. The basic idea of the differential quadrature method is that the derivative of a function, with respect to a space variable at a given sampling point, is approximated as a weighted linear sum of the sampling points in the domain of that variable. In order to illustrate the DQ approximation, consider a function $f(\zeta, \eta)$ defined on a rectangular domain $0 \leq \zeta \leq a$ and $0 \leq \eta \leq b$. Let in the given domain, the function values be known or desired on a grid of sampling points. According to DQ method, the r th derivative of the function $f(\zeta, \eta)$ can be approximated as

$$\frac{\partial^r f(\xi, \eta)}{\partial \xi^r} \Big|_{(\xi, \eta) = (\xi_i, \eta_j)} = \sum_{m=1}^{N_\xi} A_{im}^{\xi(r)} f(\xi_m, \eta_j) = \sum_{m=1}^{N_\xi} A_{im}^{\xi(r)} f_{mj} \tag{22}$$

for $i=1, 2, \dots, N_\xi; r=1, 2, \dots, N_\xi-1$

from this equation one can deduce that the important components of DQ approximations are the weighting coefficients ($A_{ij}^{\xi(r)}$) and the choice of sampling points. In order to determine the weighting coefficients a set of test functions should be used in Eq. (22). The weighting coefficients for the first-order derivatives in ξ - direction are thus determined as (Bert and Malik 1996)

$$A_{ij}^\xi = \begin{cases} \frac{1}{a} \frac{M(\xi_i)}{(\xi_i - \xi_j)M(\xi_j)} & \text{for } i \neq j \\ -\sum_{\substack{j=1 \\ i \neq j}}^{N_\xi} A_{ij}^\xi & \text{for } i = j \end{cases} ; i, j = 1, 2, \dots, N_\xi \tag{23}$$

where

$$M(\xi_i) = \prod_{j=1, j \neq i}^{N_\xi} (\xi_i - \xi_j) \tag{24}$$

The weighting coefficients of the second-order derivative can be obtained as the matrix form (Bert and Malik 1996)

$$[B_{ij}^\xi] = [A_{ij}^\xi] [A_{ij}^\xi] = [A_{ij}^\xi]^2 \tag{25}$$

In a similar manner, the weighting coefficients for the η -direction can be obtained.

It was demonstrated that non-uniform grid points gives a better result with the same number of equally spaced grid points (Bert and Malik 1996). It is shown (Shu and Wang 1999) that one of the best options for obtaining grid points is Chebyshev-Gauss-Lobatto quadrature points

$$\frac{\xi_i}{a} = \frac{1}{2} \left\{ 1 - \cos \left[\frac{(i-1)\pi}{(N_\xi - 1)} \right] \right\}, \frac{\eta_j}{b} = \frac{1}{2} \left\{ 1 - \cos \left[\frac{(j-1)\pi}{(N_\eta - 1)} \right] \right\} \tag{26a, b}$$

for $i=1, 2, \dots, N_\xi; j=1, 2, \dots, N_\eta$

By using the geometrical periodicity of the plate, the displacement components for the free vibration analysis can be represented as

$$\begin{aligned} u_r(r, \theta, z, t) &= u_{rm}(r, z) \sin(m\pi\theta/\alpha) e^{i\omega t} \\ u_\theta(r, \theta, z, t) &= u_{\theta m}(r, z) \cos(m\pi\theta/\alpha) e^{i\omega t} \\ u_z(r, \theta, z, t) &= u_{zm}(r, z) \sin(m\pi\theta/\alpha) e^{i\omega t} \end{aligned} \tag{27}$$

where $m(=0, 1, \dots, \infty)$ is the circumferential wave number; ω is the natural frequency and $i (= \sqrt{-1})$ is the imaginary number. At this stage, the DQM rules are employed to discretize the free vibration

equations and the related boundary conditions. By substituting for the displacement components from Eq. (27) and then using the DQM rules for the spatial derivatives, the discretized form of the equations of motion at each domain grid point (r_j, z_k) with $(j=2, 3, \dots, N_r-1)$ and $(k=2, 3, \dots, N_z-1)$ can be obtained as

Eq. (14)

$$\begin{aligned}
& (c_{11})_{jk} \sum_{n=1}^{N_r} B_{jn}^r u_{rmnk} + (c_{12})_{jk} \left(\frac{m\pi}{r_j^2 \alpha} u_{\theta mjk} - \frac{m\pi}{r_j \alpha} \sum_{n=1}^{N_r} A_{jn}^r u_{\theta mnk} + \frac{1}{r_j} \sum_{n=1}^{N_r} A_{jn}^r u_{rmnk} - \right. \\
& \left. \frac{1}{r_j} u_{rmnk} \right) + (c_{13})_{jk} \sum_{n=1}^{N_r} \sum_{r=1}^{N_z} A_{jn}^r A_{kr}^z u_{zmnr} + \left(\frac{\partial c_{11}}{\partial r} \right)_{jk} \sum_{n=1}^{N_r} A_{jn}^r u_{rmnk} + \left(\frac{\partial c_{12}}{\partial r} \right)_{jk} \left(\frac{1}{r_j} u_{rmjk} \right. \\
& \left. - \frac{1}{r_j} \left(\frac{m\pi}{\alpha} \right) u_{\theta mjk} \right) + \left(\frac{\partial c_{13}}{\partial r} \right)_{jk} \sum_{n=1}^{N_r} A_{kn}^z u_{zmjn} + \frac{(c_{66})_{jk}}{r_j} \left(-\frac{m\pi}{\alpha} \sum_{n=1}^{N_r} A_{jn}^r u_{\theta mnk} - \frac{m^2 \pi^2}{r_j \alpha^2} \right. \\
& \left. u_{rmjk} + \frac{m\pi}{r_j \alpha} u_{\theta mjk} \right) + \left(\frac{\partial c_{55}}{\partial z} \right)_{jk} \left(\sum_{n=1}^{N_r} A_{kn}^z u_{rmjn} + \sum_{n=1}^{N_r} A_{jn}^r u_{zmnk} \right) + (c_{55})_{jk} \left(\sum_{n=1}^{N_z} B_{kn}^z u_{rmjn} \right. \\
& \left. + \sum_{n=1}^{N_r} \sum_{r=1}^{N_z} A_{jn}^r A_{kr}^z u_{zmnr} \right) + \frac{1}{r_j} \left((c_{11})_{jk} \sum_{n=1}^{N_r} A_{jn}^r u_{rmnk} + (c_{12})_{jk} \left(\frac{-m\pi}{r_j \alpha} u_{\theta mjk} + \frac{1}{r_j} u_{rmjk} \right) \right. \\
& \left. + (c_{13})_{jk} \sum_{n=1}^{N_z} A_{kn}^z u_{zmjn} - (c_{12})_{jk} \sum_{n=1}^{N_r} A_{jn}^r u_{rmnk} - (c_{22})_{jk} \left(\frac{-m\pi}{r_j \alpha} u_{\theta mjk} + \frac{1}{r_j} u_{rmjk} \right) - \right. \\
& \left. (c_{23})_{jk} \sum_{n=1}^{N_z} A_{kn}^z u_{zmjn} \right) = -\omega_m^2 \rho_{jk} u_{rmjk}
\end{aligned} \tag{28}$$

Eq. (15)

$$\begin{aligned}
& (c_{66})_{jk} \left(\sum_{n=1}^{N_r} B_{jn}^r u_{\theta mnk} - \frac{m\pi}{r_j^2 \alpha} u_{rmjk} + \frac{m\pi}{r_j \alpha} \sum_{n=1}^{N_r} A_{jn}^r u_{rmnk} + \frac{1}{r_j} u_{\theta mjk} - \frac{1}{r_j} \sum_{n=1}^{N_r} A_{jn}^r u_{\theta mnk} \right) + \\
& \left(\frac{\partial c_{66}}{\partial r} \right)_{jk} \left(\frac{m\pi}{r_j \alpha} u_{rmjk} + \sum_{n=1}^{N_r} A_{jn}^r u_{\theta mnk} - \frac{1}{r_j} u_{\theta mjk} \right) + \frac{1}{r_j} \left((c_{12})_{jk} \frac{m\pi}{\alpha} \sum_{n=1}^{N_r} A_{jn}^r u_{rmnk} + (c_{22})_{jk} \right. \\
& \left. \left(-\frac{m^2 \pi^2}{r_j \alpha^2} u_{\theta mjk} + \frac{m\pi}{r_j \alpha} u_{rmjk} \right) + (c_{23})_{jk} \frac{m\pi}{\alpha} \sum_{n=1}^{N_z} A_{kn}^z u_{zmjn} \right) + (c_{44})_{jk} \left(\frac{m\pi}{r_j \alpha} \sum_{n=1}^{N_z} A_{kn}^z u_{zmjn} + \right. \\
& \left. \sum_{n=1}^{N_z} B_{kn}^z u_{\theta mjn} \right) + \left(\frac{\partial c_{44}}{\partial z} \right)_{jk} \left(\frac{m\pi}{r_j \alpha} u_{zmjk} + \sum_{n=1}^{N_z} A_{kn}^z u_{\theta mjn} \right) + \frac{2(c_{66})_{jk}}{r_j} \left(\sum_{n=1}^{N_r} A_{jn}^r u_{\theta mnk} + \frac{m\pi}{r_j \alpha} \right. \\
& \left. u_{rmjk} - \frac{u_{\theta mjk}}{r_j} \right) = -\omega_m^2 \rho_{jk} u_{\theta mjk}
\end{aligned} \tag{29}$$

Eq. (16)

$$\begin{aligned}
& (c_{55})_{jk} \left(\sum_{n=1}^{N_r} \sum_{r=1}^{N_z} A_{kr}^z A_{jn}^r u_{rnmr} + \sum_{n=1}^{N_r} B_{jn}^r u_{zmnk} \right) + \frac{(c_{44})_{jk}}{r_j} \left(-\frac{m^2 \pi^2}{r_j \alpha^2} u_{zmjk} - \frac{m\pi}{\alpha} \sum_{n=1}^{N_z} A_{kn}^z u_{\theta mjn} \right) + \\
& \left(\frac{\partial c_{55}}{\partial r} \right)_{jk} \left(\sum_{n=1}^{N_z} A_{kn}^z u_{rmjn} + \sum_{n=1}^{N_r} A_{jn}^r u_{zmnk} \right) + (c_{13})_{jk} \sum_{n=1}^{N_r} \sum_{r=1}^{N_z} A_{kr}^z A_{jn}^r u_{rnmr} + (c_{23})_{jk} \left(\frac{-m\pi}{r_j \alpha} \sum_{n=1}^{N_z} A_{kn}^z u_{\theta mjn} + \right.
\end{aligned}$$

$$\begin{aligned} & \frac{1}{r_j} \sum_{n=1}^{N_z} A_{kn}^z u_{rmjn}) + (c_{33})_{jk} \sum_{n=1}^{N_z} B_{kn}^z u_{zmjn} + \left(\frac{\partial c_{13}}{\partial z}\right)_{jk} \sum_{n=1}^{N_r} A_{jn}^r u_{rmnk} + \left(\frac{\partial c_{23}}{\partial z}\right)_{jk} \left(\frac{-m\pi}{r_j \alpha} u_{\theta mj} + \frac{u_{rmjk}}{r_j}\right) + \\ & \left(\frac{\partial c_{33}}{\partial z}\right)_{jk} \sum_{n=1}^{N_z} A_{kn}^z u_{zmjn} + \frac{(c_{55})_{jk}}{r_j} \left(\sum_{n=1}^{N_z} A_{kn}^z u_{rmjn} + \sum_{n=1}^{N_r} A_{jn}^r u_{zmnk}\right) = -\omega_m^2 \rho_{jk} u_{zmjk} \end{aligned} \tag{30}$$

where A_{ij}^r, A_{ij}^z and B_{ij}^r, B_{ij}^z are the first and second order DQ weighting coefficients in the r - and z - directions, respectively.

In a similar manner, the boundary conditions can be discretized. For this purpose, using Eq. (27) and the DQM discretization rules for spatial derivatives, the boundary conditions at $z=-h/2$ and $h/2$ become,

Eq. (17)
at $z = -h/2$

$$\begin{aligned} & \sum_{n=1}^{N_z} A_{kn}^z u_{rmjn} + \sum_{n=1}^{N_r} A_{jn}^r u_{zmnk} = 0, \frac{m\pi}{r_j \alpha} u_{zmjk} + \sum_{n=1}^{N_z} A_{kn}^z u_{\theta mjn} = 0, \\ & (c_{13})_{jk} \sum_{n=1}^{N_r} A_{jn}^r u_{rmnk} + (c_{23})_{jk} \left(\frac{1}{r_j} u_{rmjk} - \frac{m\pi}{r_j \alpha} u_{\theta mj}\right) + (c_{33})_{jk} \sum_{n=1}^{N_z} A_{kn}^z u_{zmjn} \\ & -K_w u_{zmjk} + K_g \left(\sum_{n=1}^{N_r} B_{jn}^r u_{zmnk} + \frac{1}{r_j} \sum_{n=1}^{N_r} A_{jn}^r u_{zmnk} - \frac{m^2 \pi^2}{r_j^2 \alpha^2} u_{zmjk}\right) = 0 \end{aligned} \tag{31}$$

Eq. (18)
at $z = h/2$

$$\begin{aligned} & \sum_{n=1}^{N_z} A_{kn}^z u_{rmjn} + \sum_{n=1}^{N_r} A_{jn}^r u_{zmnk} = 0, \frac{m\pi}{r_j \alpha} u_{zmjk} + \sum_{n=1}^{N_z} A_{kn}^z u_{\theta mjn} = 0, \\ & (c_{13})_{jk} \sum_{n=1}^{N_r} A_{jn}^r u_{rmnk} + (c_{23})_{jk} \left(\frac{1}{r_j} u_{rmjk} - \frac{m\pi}{r_j \alpha} u_{\theta mj}\right) + (c_{33})_{jk} \sum_{n=1}^{N_z} A_{kn}^z u_{zmjn} = 0 \end{aligned} \tag{32}$$

where $k=1$ at $z=0$ and $k=N_z$ at $z=h$, and $j=1, 2, \dots, N_r$.
The boundary conditions at $r=b$ and a stated in Eqs. (19)-(21) become,
-Simply supported(S)

$$\begin{aligned} & u_{\theta mj} = 0, u_{zmjk} = 0, \\ & (c_{11})_{jk} \sum_{n=1}^{N_r} A_{jn}^r u_{rmnk} + (c_{12})_{jk} \left(\frac{-m\pi}{r_j \alpha} u_{\theta mj} + \frac{1}{r_j} u_{rmjk}\right) + (c_{13})_{jk} \sum_{n=1}^{N_z} A_{kn}^z u_{zmjn} = 0 \end{aligned} \tag{33a}$$

-Free (F)

$$\begin{aligned} & (c_{11})_{jk} \sum_{n=1}^{N_r} A_{jn}^r u_{rmnk} + (c_{12})_{jk} \left(\frac{-m\pi}{r_j \alpha} u_{\theta mj} + \frac{1}{r_j} u_{rmjk}\right) + (c_{13})_{jk} \sum_{n=1}^{N_z} A_{kn}^z u_{zmjn} = 0, \\ & \sum_{n=1}^{N_r} A_{jn}^r u_{\theta mnk} + \frac{m\pi}{r_j \alpha} u_{rmjk} - \frac{1}{r_j} u_{\theta mj} = 0, \end{aligned}$$

$$\sum_{n=1}^{N_z} A_{kn}^z u_{rmjn} + \sum_{n=1}^{N_r} A_{jn}^r u_{zmnk} = 0 \quad (33b)$$

-Clamped(C)

$$u_{rmjk} = 0, u_{\theta mj} = 0, u_{z mj} = 0 \quad (33c)$$

In the above equations $k=2, \dots, N_z-1$; also $j=1$ at $r=b$ and $j=N_r$ at $r=a$.

In order to carry out the eigenvalue analysis, the domain and boundary degrees of freedom are separated and in vector forms, they are denoted as $\{d\}$ and $\{b\}$, respectively. Based on this definition, the discretized form of the equilibrium equations and the related boundary conditions take the following forms,

Equations of motion (28)-(30)

$$\left[\begin{matrix} [K_{db}] \\ [K_{dd}] \end{matrix} \right] \begin{Bmatrix} \{b\} \\ \{d\} \end{Bmatrix} - \omega^2 [M] \{d\} = \{0\} \quad (34)$$

Boundary conditions Eqs. (31)-(32) and Eq. (33a, b and c)

$$[K_{bd}] \{d\} + [K_{bb}] \{b\} = \{0\} \quad (35)$$

Eliminating the boundary degrees of freedom in Eq. (34), using Eq. (35), this equation becomes

$$[K] - \omega^2 [M] \{d\} = \{0\} \quad (36)$$

where $[K] = [K_{dd}] - [K_{db}] [K_{bb}]^{-1} [K_{bd}]$. The above eigenvalue system of equations can be solved to find the natural frequencies and mode shapes of the plates.

6. Numerical results and discussion

In this section, the convergence behavior of the method is investigated and comparisons with other available solutions are made to verify the accuracy of the results. Then, the effects of the different geometrical parameters, the material properties and coefficients of elastic foundation on the free vibration characteristics of FG annular sector plates are presented.

As a first example, the comparative studies of the fundamental frequency parameters are given in Table 2. It is seen from Table 2 that for thin plates ($h/a=0.01$) there is an excellent agreement between the present 3-D solutions and the classical solutions. For moderately thick plates, ($h/a=0.2$) the present 3-D solutions also agree quite well with the Mindlin solutions. For very thick plates ($h/a=0.4$) the discrepancies increase, particularly for C-C plates. It is found that only nineteen DQ grid points in each direction (r and z) can yield accurate results. The same problem has been analyzed by Zhou *et al.* (2009). It is obvious that the error of the Mindlin plate theory increases with the increase of the plate thickness, especially for very thick plates ($h/a \geq 0.4$). The two-dimensional theories, such as the classical plate theory, the first- and the higher- order shear deformation plate theories neglect transverse normal deformations, and generally assume that a plane stress state of deformation prevails in the plate. These assumptions may be appropriate for thin plates but do not give good results for thick plates. It is seen from Table 2 that the maximum

Table 2 Comparison of fundamental frequency parameter ($\Omega = \omega a^2 \sqrt{\rho h/D}$) for flexural vibration of annular sector plates with two straight edges simply supported ($b/a=0.5$)

α (deg)	h/a	Theories	C-C	F-C	F-S
195	0.01	(McGee <i>et al.</i> 1995)	90.0837	21.4263	10.8761
		(Zhou <i>et al.</i> 2009)	90.1125	21.4074	10.8522
		Present ($N_r=N_z=9$)	90.1102	21.4065	10.8513
		Present ($N_r=N_z=13$)	90.1124	21.4075	10.8520
		Present ($N_r=N_z=17$)	90.1122	21.4076	10.8525
		Present ($N_r=N_z=19$)	90.1123	21.4076	10.8524
	0.2	(McGee <i>et al.</i> 1995)	70.8090	19.9986	10.2268
		(Zhou <i>et al.</i> 2009)	71.9146	20.0967	10.2386
		Present ($N_r=N_z=9$)	71.9115	20.0954	10.2392
		Present ($N_r=N_z=13$)	71.9142	20.0964	10.2380
		Present ($N_r=N_z=17$)	71.9143	20.0968	10.2385
		Present ($N_r=N_z=19$)	71.9143	20.0968	10.2384
	0.4	(McGee <i>et al.</i> 1995)	48.6618	17.5822	9.3661
		(Zhou <i>et al.</i> 2009)	50.0059	17.7636	9.3961
		Present ($N_r=N_z=9$)	50.0045	17.7653	9.3945
		Present ($N_r=N_z=13$)	50.0059	17.7641	9.3958
		Present ($N_r=N_z=17$)	50.0056	17.7638	9.3961
		Present ($N_r=N_z=19$)	50.0056	17.7638	9.3962

Table 3 The lowest non-dimensional frequency parameter ($\varpi = \omega h \sqrt{\rho/C_{11}}$) for FGMs annular sector plates having clamped ($r=b$) and clamped ($r=a$) conditions ($h/a=0.1$)

α (deg)	b/a	m		λ				
				1	2	3	4	5
195	0.1	1	(Nie and Zhong 2008)	0.0663	0.0622	0.0566	0.0505	0.0446
			Present ($N_r=N_z=9$)	0.0651	0.0611	0.0553	0.0497	0.0432
			Present ($N_r=N_z=13$)	0.0661	0.0620	0.0561	0.0502	0.0440
			Present ($N_r=N_z=17$)	0.0664	0.0622	0.0564	0.0505	0.0444
			Present ($N_r=N_z=19$)	0.0664	0.0623	0.0564	0.0505	0.0445
		2	(Nie and Zhong 2008)	0.0795	0.0746	0.0677	0.0603	0.0531
			Present ($N_r=N_z=9$)	0.0781	0.0712	0.0666	0.0589	0.0519
			Present ($N_r=N_z=13$)	0.0791	0.0743	0.0677	0.0601	0.0528
			Present ($N_r=N_z=17$)	0.0793	0.0746	0.0679	0.0604	0.0530
			Present ($N_r=N_z=19$)	0.0793	0.0747	0.0679	0.0603	0.0530
	0.3	1	(Nie and Zhong 2008)	0.1041	0.0980	0.0895	0.0801	0.0710
			Present ($N_r=N_z=9$)	0.1049	0.0968	0.0888	0.0789	0.0721
			Present ($N_r=N_z=13$)	0.1041	0.0981	0.0896	0.0801	0.0712
			Present ($N_r=N_z=17$)	0.1039	0.0979	0.0898	0.0799	0.0710
		2	(Nie and Zhong 2008)	0.1104	0.1039	0.0948	0.0849	0.0753
			Present ($N_r=N_z=9$)	0.1094	0.1030	0.0933	0.0839	0.0741
			Present ($N_r=N_z=13$)	0.1103	0.1038	0.0946	0.0845	0.0755
			Present ($N_r=N_z=17$)	0.1106	0.1040	0.0950	0.0850	0.0751
		Present ($N_r=N_z=19$)	0.1105	0.1039	0.0950	0.0850	0.0752	

Table 4 The lowest non-dimensional frequency parameter ($\omega = \omega h \sqrt{\rho/C_{11}}$) for FGMs annular sector plates having clamped ($r=b$) and simply supported ($r=a$) conditions ($h/a=0.1$)

α (deg)	b/a	m		λ				
				1	2	3	4	5
195	0.1	1	(Nie and Zhong 2008)	0.0442	0.0412	0.0372	0.0329	0.0289
			Present ($N_r=N_z=9$)	0.0431	0.0429	0.0361	0.0319	0.0271
			Present ($N_r=N_z=13$)	0.0440	0.0417	0.0370	0.0336	0.0282
			Present ($N_r=N_z=17$)	0.0444	0.0412	0.0376	0.0331	0.0287
			Present ($N_r=N_z=19$)	0.0444	0.0411	0.0374	0.0329	0.0287
		2	(Nie and Zhong 2008)	0.0582	0.0542	0.0488	0.0431	0.0377
			Present ($N_r=N_z=9$)	0.0594	0.0559	0.0477	0.0441	0.0362
			Present ($N_r=N_z=13$)	0.0588	0.0549	0.0483	0.0433	0.0372
			Present ($N_r=N_z=17$)	0.0584	0.0543	0.0487	0.0430	0.0376
			Present ($N_r=N_z=19$)	0.0584	0.0544	0.0487	0.0429	0.0378
	0.3	1	(Nie and Zhong 2008)	0.0727	0.0680	0.0617	0.0548	0.0484
			Present ($N_r=N_z=9$)	0.0710	0.0689	0.0605	0.0538	0.0495
			Present ($N_r=N_z=13$)	0.0717	0.0685	0.0611	0.0544	0.0488
			Present ($N_r=N_z=17$)	0.0721	0.0682	0.0615	0.0548	0.0485
			Present ($N_r=N_z=19$)	0.0726	0.0682	0.0618	0.0548	0.0485
		2	(Nie and Zhong 2008)	0.0802	0.0751	0.0695	0.0604	0.0532
			Present ($N_r=N_z=9$)	0.0790	0.0741	0.0690	0.0619	0.0546
			Present ($N_r=N_z=13$)	0.0797	0.0754	0.0684	0.0613	0.0536
			Present ($N_r=N_z=17$)	0.0800	0.0750	0.0680	0.0607	0.0533
			Present ($N_r=N_z=19$)	0.0803	0.0750	0.0680	0.0605	0.0531

Table 5 Mechanical properties of the materials

	<i>Cu</i>	<i>W</i>
E (GPa)	115.0	400.0
ν	0.31	0.28
ρ (kg/m ³)	8960	19,300

differences between the 3-D solutions and the Mindlin solutions occur at the Clamped-Clamped plates.

As the second example, the convergence behavior and accuracy of the method for lowest non-dimensional frequency parameter of thick FG annular sector plates with two different sets of circular edge conditions including Clamped-Clamped and Clamped-Simply supported are studied in Tables 3 and 4. The results are compared with those of the three-dimensional elasticity solutions of Nie and Zhong (2008) which are obtained by using the state space method. It is assumed that the material properties vary exponentially ($c_{ij}(z) = c_{ij}^M e^{(\lambda z/h)}$, $\rho(z) = \rho^M e^{(\lambda z/h)}$) through the thickness of the plate. Superscripts M denote the material properties of the bottom surface of the plate, λ is the material property graded index. One can see that an excellent agreement exists between the converged results of the presented approach and the other one. A numerical value of $N_r=N_z=19$ is used for the next studies.

In this section, we characterize the response of CGFR plate with graded fiber volume fractions

in the plate’s thickness on elastic foundations. The CGFR plate consists of continuous tungsten reinforcement fibers in a copper matrix (W/Cu). The relevant material properties for the constituent materials are listed in Table 5. Here we assume that the plate has a continuous variation (according to Eq. (6)), starting at $V_w=0$ (0% tungsten, 100% copper) on the lower surface of the plate to $V_w=0.75$ (75% tungsten, 25% copper) on the upper surface. The non-dimensional natural frequency, Winkler and shearing layer elastic coefficients are as follows

$$\Omega = \omega a^2 \sqrt{\rho_i h / D_i} \quad , \quad D_i = E_i h^3 / 12(1 - \nu_i^2),$$

$$k_g = K_g a^2 / D_i \quad , \quad k_w = K_w a^4 / D_i$$
(37)

Where ρ_i , E_i and ν_i are mechanical properties of 100% copper.

The influence of constituent volume fractions is studied by varying the volume fractions of W/Cu. This is carried out by varying the power-law exponent “ p ”. Figs. 4 and 5 show the influence of the constituent volume fractions “ p ” on the first two non-dimensional natural frequencies of the CGFR plates on an elastic foundation.

It is observed with increasing power-law exponent “ p ” (decreasing volume fraction of Tungsten fiber) the first two non-dimensional natural frequencies decrease sharply for small value of “ p ” ($p < 1$) and then for $p > 15$ it reaches a constant value for different values of the shearing layer elastic coefficient. It should be noted that second derivative of the curves in Fig. 2 is positive for $p < 1$ and negative for $p > 1$. It is obvious for $p = 1$, the second derivative is equal to zero. Therefore, in Figs. 4 and 5 the curves have a first decreasing branch, followed by an increasing part, and finally they become constant for $p > 15$, because the volume fraction of the matrix gets approximately constant along the thickness of the plate.

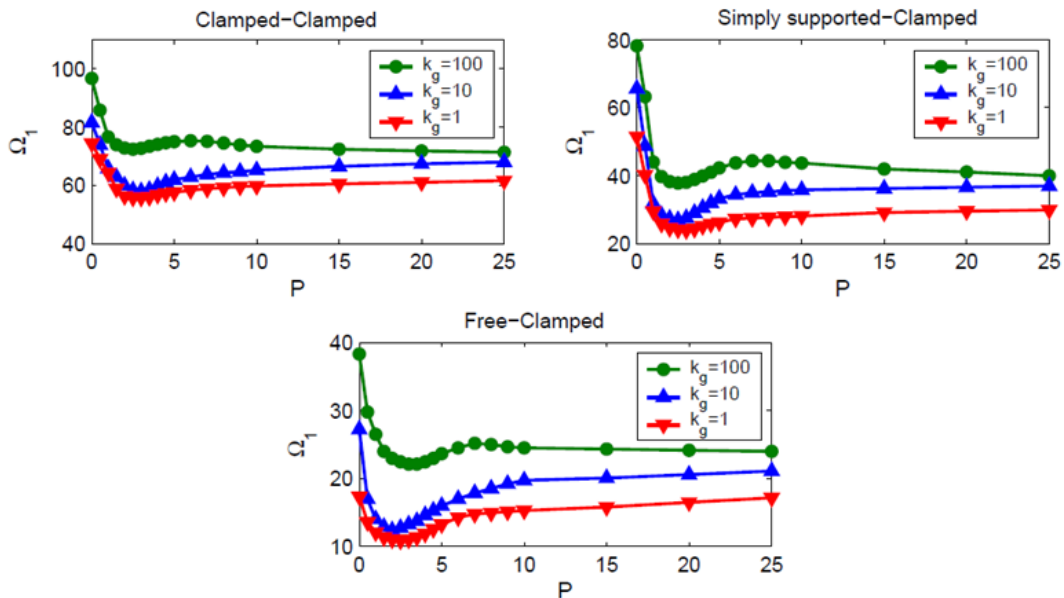


Fig. 4 Variation of the first non-dimensional natural frequency parameter of CGFR annular sector plates on a two-parameter elastic foundation versus “ p ” for different boundary conditions and shearing elastic coefficient ($K_w=100$, $h/a=0.2$, $b/a=0.2$, $\alpha=195^\circ$)

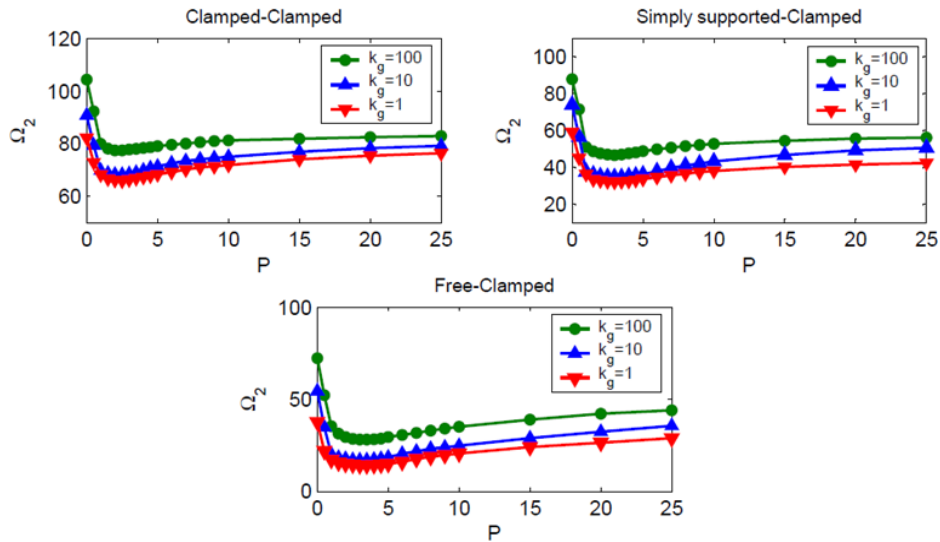


Fig. 5 Variation of the second non-dimensional natural frequency parameter of CGFR annular sector plates on a two-parameter elastic foundation versus “*p*” for different boundary conditions and shearing elastic coefficient ($K_w=100, h/a=0.2, b/a=0.2, \alpha=195^\circ$)

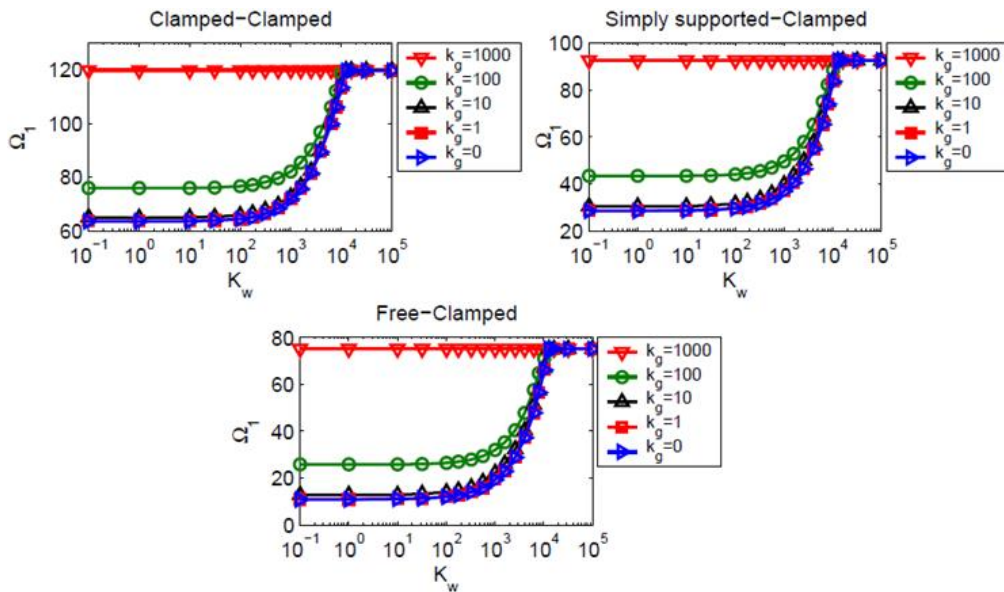


Fig. 6 Variation of the first non-dimensional natural frequency parameter of CGFR annular sector plates on a two-parameter elastic foundation versus Winkler elastic coefficient for different boundary conditions ($p=1, h/a=0.2, b/a=0.2, \alpha=195^\circ$)

The effect of Winkler elastic coefficient on the first non-dimensional natural frequency parameters at different values of shearing layer elastic coefficient with different boundary conditions including Simply supported-Clamped, Camped-Clamped and Free-Clamped is shown in Fig. 6. It is observed for the large values of Winkler elastic coefficient, the shearing layer elastic

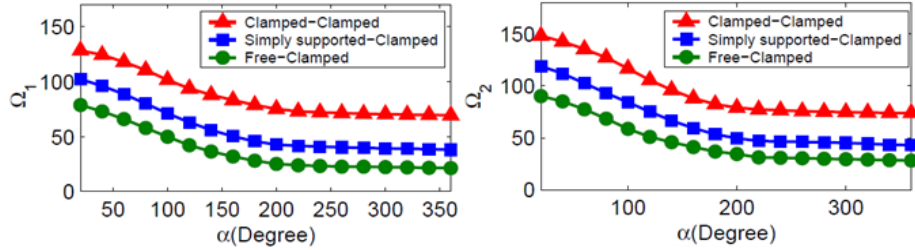


Fig. 7 The influence of the sector angle on the first and second non-dimensional natural frequency parameter of CGFR annular sector plates on elastic foundations ($K_w=K_g=100$, $b/a=h/a=0.2$, $p=1$)

Table 6 Material volume fractions of 2-layer, 3-layer and CGFR plates

Type of Plates		Material volume fractions
2 Layers	1 st lamina	0% Tungsten, 100% copper
	2 st lamina	75% Tungsten, 25% copper
3 Layers	1 st lamina	0% Tungsten, 100% copper
	2 st lamina	37.5% Tungsten, 62.5% copper
	3 st lamina	75% Tungsten, 25% copper
CGFR	Bottom surface	0% Tungsten, 100% copper
	Top surface	75% Tungsten, 25% copper

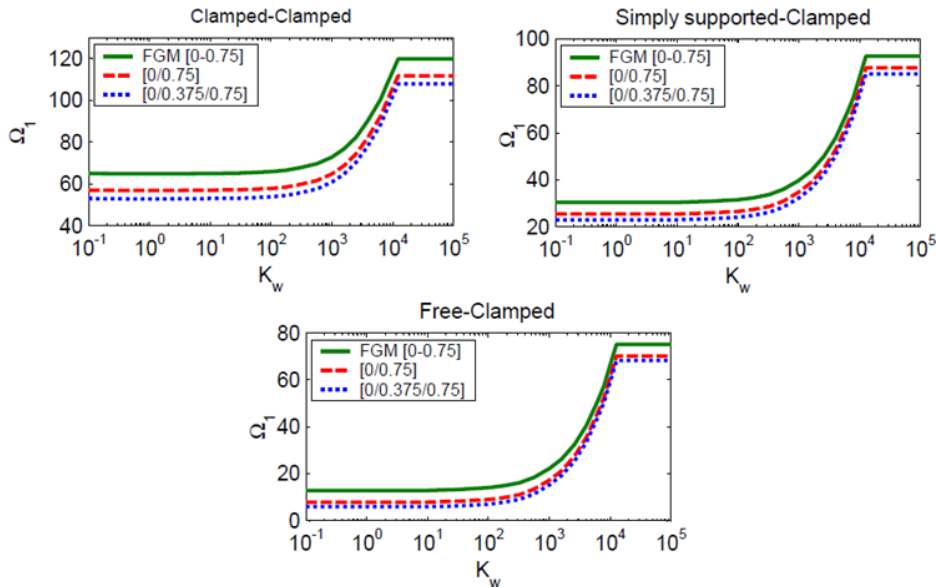


Fig. 8 The effect of Winkler elastic coefficients on the first non-dimensional natural frequency parameter of CGFR, 2-layer and 3-layer annular sector plates ($K_g=10$, $b/a=h/a=0.2$, $p=1$, $\alpha=195^\circ$)

coefficient has less effect and the results become independent of it. In other word, the non-dimensional natural frequency parameters converge with increasing Winkler elastic coefficient of the foundation. It can be concluded from Fig. 6 that the non-dimensional natural frequency parameters converge at the large values of Winkler elastic coefficient. The influences of the sector

angle on the fundamental frequency parameter of CGFR annular sector plates on a two-parameter elastic foundation with different circular edge conditions are shown in Fig. 7.

It is obvious that by increasing the sector angle, the frequency parameter decreases. Now we turn our attention to the comparison of the CGFR plate with discretely laminated 2-layer, 3-layer plate containing [0/0.75], [0/0.375/0.75] volume fractions, respectively, as shown in Table 6. Figs. 8 and 9 demonstrate how the first and second non-dimensional natural frequencies benefit from a gradual change in volume fraction from the lower surface to the upper one. According to these figures, the first and second non-dimensional natural frequencies of the CGFR plate increase in comparison with similar discrete laminated plates on a two-parameter elastic foundation.

For an overall comprehension on 3-D vibration of CGFR annular sector plates, some mode shape contour plots are depicted in Figs. 10, 11 and 12. Now we consider the non-dimensional natural frequency as

$$\lambda = \omega a^2 \sqrt{\rho_{Al} h / D_{Al}} \quad , \quad D_{Al} = E_{Al} h^3 / 12(1 - \nu_{Al}^2) \quad , \quad k_g = K_g a^2 / D_{Al} \quad , \quad k_w = K_w a^4 / D_{Al} \quad (38)$$

Where ρ_{Al} , E_{Al} and ν_{Al} are mechanical properties of aluminum.

It should be noted that the isotropic 2-D FGM sector plates considered in this work, are assumed to be composed of aluminum and silicon carbide. In the following, we have compared several different ceramic volume fraction profiles of conventional 1-D and 2-D FGMs with appropriate choice of the radial and thickness parameters of the 2-D six-parameter power-law distribution, as shown in Table 7. It should be noted that the notation Classical-Symmetric indicates that the 2-D FGM annular sector plate has Classical and Symmetric volume fraction profiles in the radial and thickness directions, respectively.

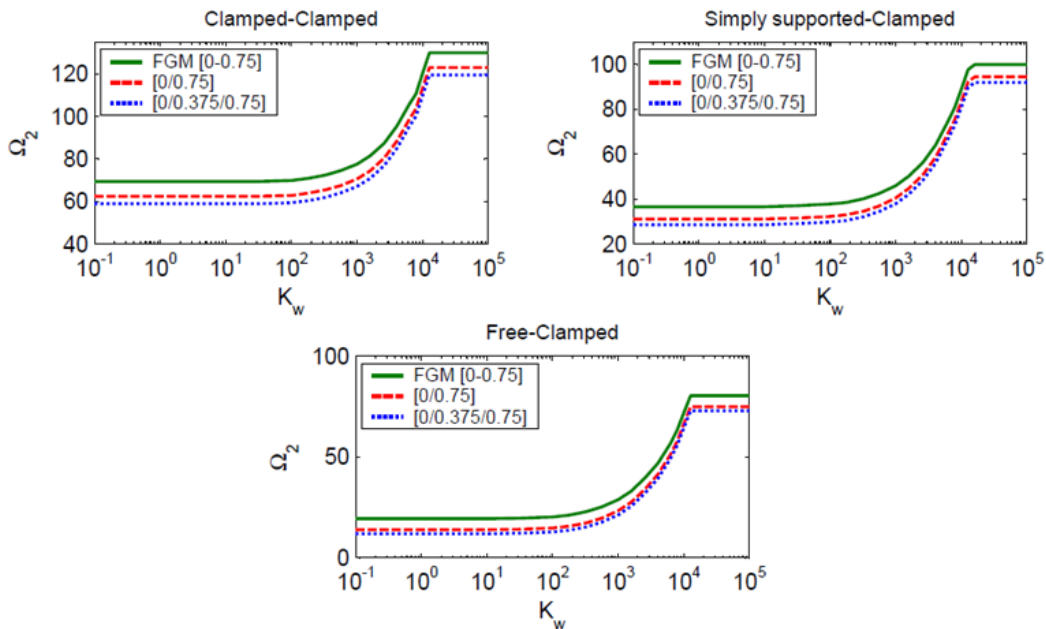


Fig. 9 The effect of Winkler elastic coefficients on the second non-dimensional natural frequency parameter of CGFR, 2-layer and 3-layer annular sector plates ($K_g=10, b/a=h/a=0.2, p=1, \alpha=195^\circ$)

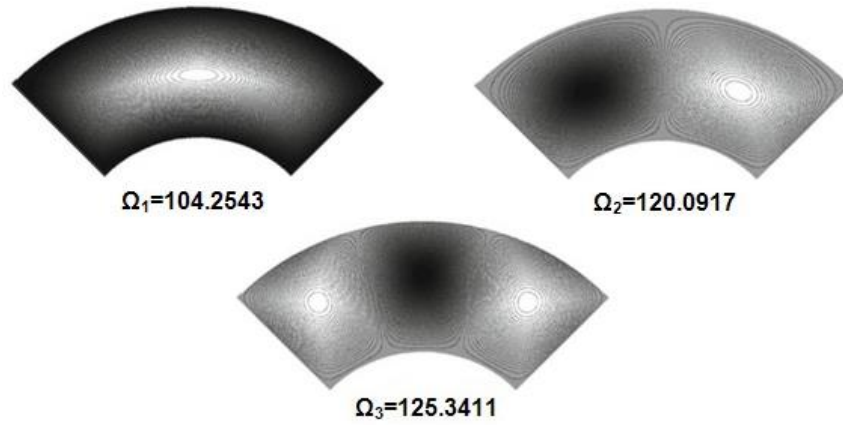


Fig. 10 Mode shape plots of the CGFR annular sector plates with Clamped-Clamped boundary conditions at the circular edges ($K_w=K_g=100$, $b/a=h/a=0.2$, $p=1$, $\alpha=195^\circ$)

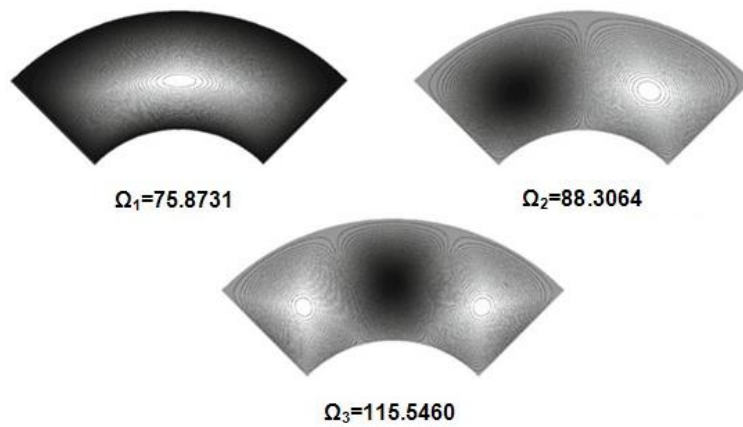


Fig. 11 Mode shape plots of the CGFR annular sector plates with Simply supported-Clamped boundary conditions at the circular edges ($K_w=K_g=100$, $b/a=h/a=0.2$, $p=1$, $\alpha=90^\circ$)

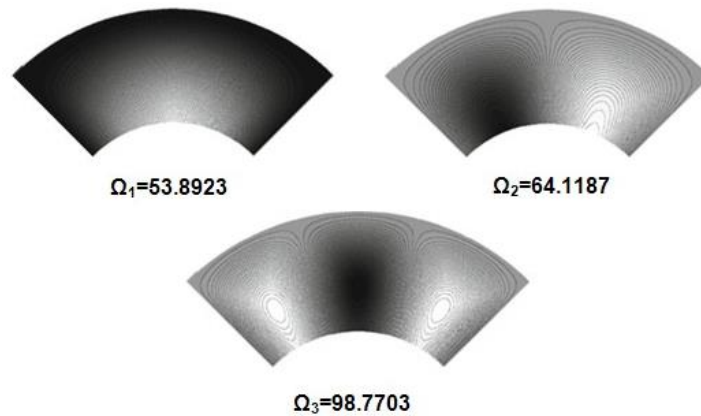


Fig. 12 Mode shape plots of the CGFR annular sector plates with Free-Clamped boundary conditions at the circular edges ($K_w=K_g=100$, $b/a=h/a=0.2$, $p=1$, $\alpha=90^\circ$)

Table 7 Various ceramic volume fraction profiles, different parameters, and volume fraction indices of 2-D power-law distributions

Volume fraction profile	Radial volume fraction Index and parameters	The volume fraction of Thickness, Index and parameters
Classical-Classical	$\alpha_r=0$	$\alpha_z=0$
Symmetric-Symmetric	$\alpha_r=1, \beta_r=2$	$\alpha_z=1, \beta_z=2$
Classical- Symmetric	$\alpha_r=0$	$\alpha_z=1, \beta_z=2$
Classical radially	$\alpha_r=0$	$\gamma_z=0$
Symmetric radially	$\alpha_r=1, \beta_r=2$	$\gamma_z=0$

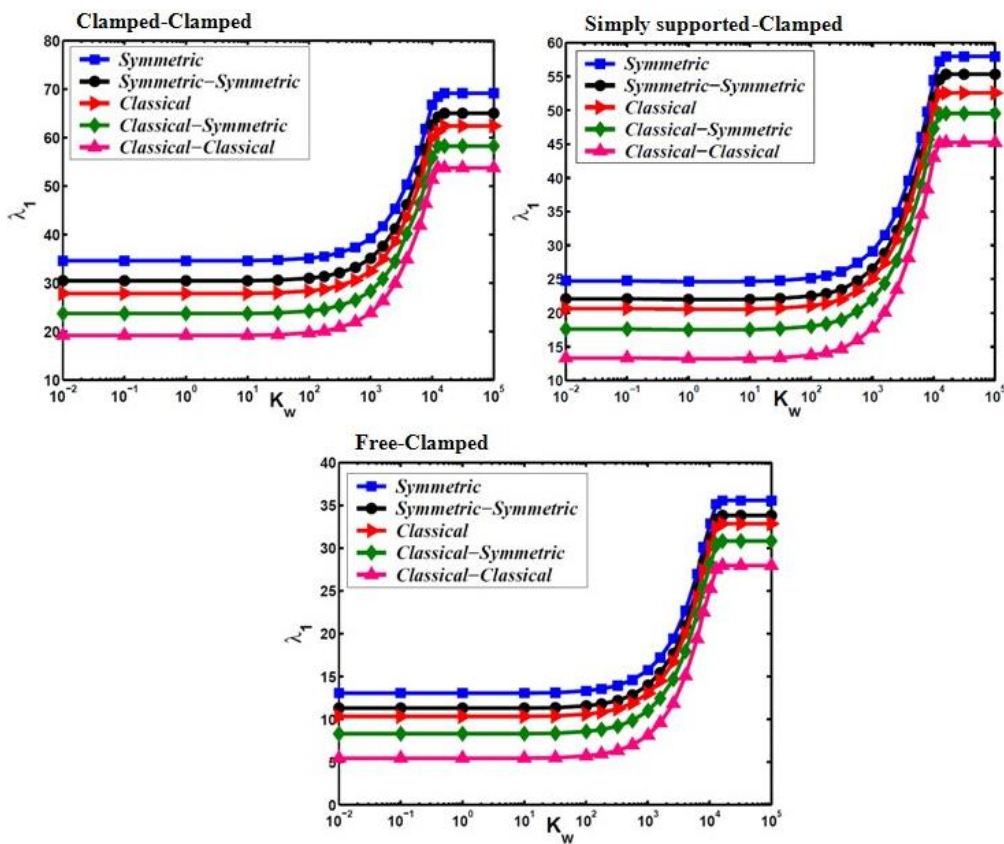


Fig. 13 Variations of fundamental frequency parameters of a bi-directional FG annular sector plate resting on a two-parameter elastic foundation with Winkler elastic coefficient for different volume fraction profiles ($K_g=100, \gamma_z=2, h/a=b/a=0.5, \alpha=195^\circ$)

The effect of the Winkler elastic coefficient on the fundamental frequency parameters of a bi-directional FG sector plate for different boundary conditions is shown in Fig. 13. According to this figure, the lowest frequency parameter is obtained by using Classical- Classical volume fraction profile. On the contrary, the 1-D FG sector plate with Symmetric volume fraction profile has the maximum value of the frequency parameter. It can be also seen from Fig. 13, for different boundary conditions, Classical-Classical volume fraction profile has the lowest frequencies

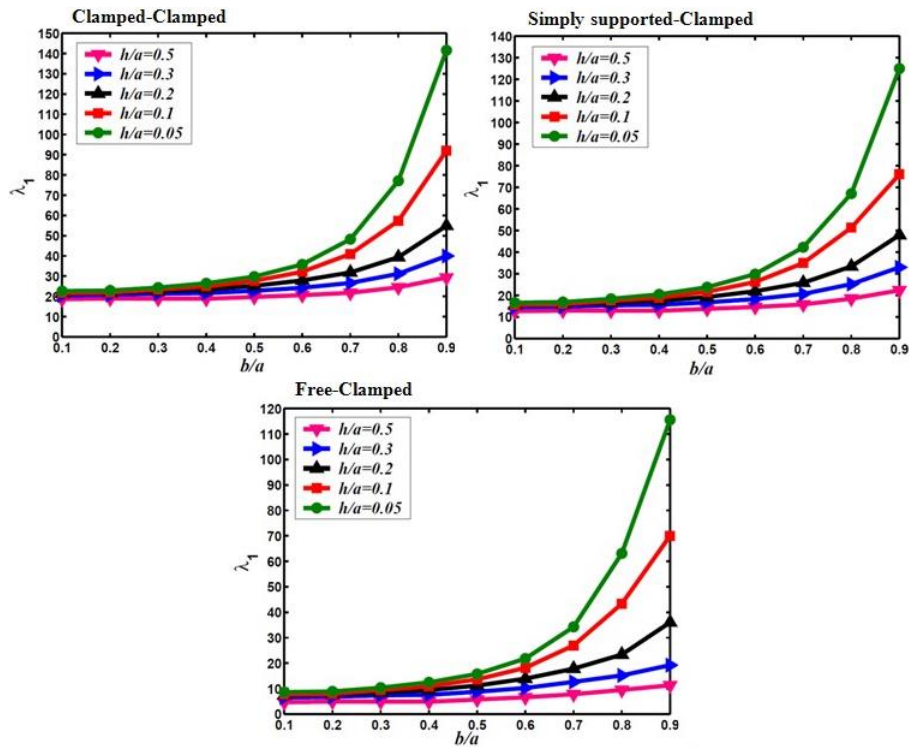


Fig. 14 Variation of fundamental frequency parameters of an elastically supported bi-directional FG annular sector plate versus b/a ratio for different boundary conditions at circular edges profiles ($K_w=K_g=100, \gamma_z=2, \alpha_r=\alpha_z=0, \alpha=195^\circ$)

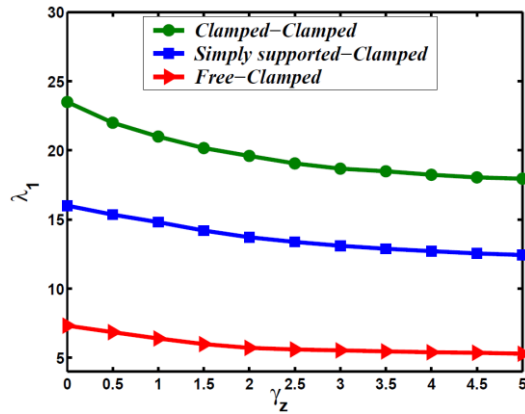


Fig. 15 Frequency variation against volume fraction index (γ_z) for a bi-directional FG annular sector plate resting on a two-parameter elastic foundation ($K_w=K_g=100, h/a=b/a=0.5, \gamma_r=2, \alpha_r=\alpha_z=0, \alpha=195^\circ$)

followed by Classical-Symmetric, Classical, Symmetric-Symmetric and Symmetric profiles. Therefore, a graded ceramic volume fraction in two directions has higher capabilities to reduce the frequency parameter than conventional 1-D FGM.

The variation of inner-outer radius ratio (b/a) with the frequency parameters of a Clamped-Clamped, Simply supported-Clamped and Free-Clamped bi-directional FG annular sector plates resting on a Pasternak elastic foundation for different values of h/a ratios is shown in Fig. 14. According to Fig. 14, the general behavior of the frequency parameters of a bi-directional FG annular sector plate for all b/a ratios is that the effects of the h/a ratios are more prominent at high inner-to-outer radius ratios. As it is observed, the frequency parameter decreases rapidly with the decrease of the b/a ratio and then remains almost unaltered for the $b/a < 0.3$.

Now we study the influence of various types of the ceramic volume fraction profile on fundamental natural frequency at various volume fraction indices through the thickness direction (γ_z) of the annular sector plates (Fig. 15). The results show that, for the all boundary conditions the frequency parameter decreases by increasing the thickness volume fraction index, due to the fact that the silicon carbide fraction decreases, and as we know silicon carbide has a much higher Young's modulus than aluminum. It is also seen, that the thickness volume fraction index has less effect on the frequency parameter for the Classical-Classical volume fraction profile.

7. Conclusions

In this research work, free vibration of continuous grading fiber reinforced (CGFR) and bi-directional FG annular sector plates on a two-parameter elastic foundation are investigated based on three-dimensional theory of elasticity. The elastic foundation is considered as a Pasternak model with adding a shear layer to the Winkler model. Three complicated equations of motion for the plate under consideration are semi-analytically solved using 2-D differential quadrature method. Using the two-dimensional differential quadrature method in the r - and z -directions, allows one to deal with FG plates with arbitrary thickness distribution of material properties and also to implement the effects of the elastic foundations as a boundary condition on the lower surface of the plate efficiently and in an exact manner. The fast rate of convergence and accuracy of the method are investigated through the different solved examples. The effects of different boundary conditions, various geometrical parameters such as the sector angle, different ceramic volume fraction profiles along the thickness and radial directions, elastic coefficients of foundation of bi-directional annular sector plates are investigated. Moreover, vibration behavior of 2-D FG plates is compared with one-dimensional conventional FG plates. From this study, some conclusions can be made:

- It is shown that with increasing the elastic coefficients of the foundation, the frequency parameters increase to some limit values. It is observed for the large values of Winkler elastic coefficient, the shearing layer elastic coefficient has less effect and the results become independent of it.
- It is observed that with increasing power-law exponent " p " (decreasing volume fraction of Tungsten fiber) the first two non-dimensional natural frequencies decrease sharply for small value of " p " and then for $p > 15$, they become constant because the volume fraction of the matrix gets approximately constant along the thickness of the plate.
- It is observed that the CGFR plate attains natural frequency higher than those of traditional discretely laminated composite ones and close to that of a 2-layer.
- It is shown that the CGFR plate attains natural frequency higher than those of traditional discretely laminated composite ones and this can be a benefit when higher stiffness of the plate is the goal and that is due to the reduction in spatial mismatch of material properties.

- The interesting results show that the lowest magnitude frequency parameter is obtained by using a Classical-Classical volume fraction profile. It can be concluded that a graded ceramic volume fraction in two directions has higher capabilities to reduce the natural frequency than a conventional 1-D FGM.
- It is also seen that the thickness volume fraction index exerts an insignificant influence on the frequency parameter for the Classical-Classical volume fraction profile.
- It is shown that the general behavior of the frequency parameters of a bi-directional FG annular sector plate for all b/a ratios is that the effects of the h/a ratios are more prominent at high inner-to-outer radius ratios. As it is observed, the frequency parameter decreases rapidly with the decrease of the b/a ratio and then remains almost unaltered for the $b/a < 0.3$.
- It is observed that for different boundary conditions, Classical-Classical volume fraction profile has the lowest frequencies followed by Classical-Symmetric, Classical, Symmetric-Symmetric and Symmetric profiles.

References

- Benveniste, Y. (1987), "A new approach to the application of Mori-Tanaka's theory of composite materials", *Mech. Mater.*, **6**(2), 147-157.
- Bert, C.W. and Malik, M. (1996), "Differential quadrature method in computational mechanics, a review", *Appl. Mech. Rev.*, **49**(1), 1-28.
- Cheng, Z.Q. and Batra, R.C. (2000), "Exact correspondence between eigenvalues of membranes and functionally graded simply supported polygonal plates", *J. Sound Vib.*, **229**(4), 879-895.
- Cheng, Z.Q. and Kitipornchai, S. (1999), "Membrane analogy of buckling and vibration of inhomogeneous plates", *J. Eng. Mech.*, **125**(11), 1293-1297.
- Hosseini-Hashemi, S., Akhavan, H., Rokni Damavandi Taher, H., Daemi, N. and Alibeigloo, A. (2010a), "Differential quadrature analysis of functionally graded circular and annular sector plates on elastic foundation", *Mater. Des.*, **31**(4), 1871-1880.
- Hosseini-Hashemi, S., Rokni Damavandi Taher, H. and Akhavan, H. (2010b), "Vibration analysis of radially FGM sectorial plates of variable thickness on elastic foundations", *Compos. Struct.*, **92**(7), 1734-1743.
- Houmat, A. (2004), "Three-dimensional hierarchical finite element free vibration analysis of annular sector plates", *J. Sound Vib.*, **276**(1-2), 181-193.
- Kim, C.S. and Dickinson, S.M. (1989), "On the free, transverse vibration of annular and circular, thin, sectorial plates subjected to certain complicating effects", *J. Sound Vib.*, **134**(3), 407-421.
- Liew, K.M. and Lam, K.Y. (1993), "On the use of 2-d orthogonal polynomials in the Rayleigh-Ritz method for flexural vibration of annular sector plates of arbitrary shape", *Int. J. Mech. Sci.*, **35**(2), 129-139.
- Liew, K.M., Ng, T.Y. and Wang, B.P. (2001), "Vibration of annular sector plates from three-dimensional analysis", *J. Acoust. Soc. Am.*, **110**(1), 233-242.
- Lü, C.F., Chen, W.Q., Xu, R.Q. and Lim, C.W. (2008), "Semi-analytical elasticity solutions for bi-directional functionally graded beams", *Int. J. Solid. Struct.*, **45**(1) 258-275.
- Lü, C.F., Lim, C.W. and Chen, W.Q. (2009), "Semi-analytical analysis for multi-directional functionally graded plates: 3-D elasticity solutions", *Int. J. Num. Meth. Eng.*, **79**(1), 25-44.
- McGee, O.G., Huang, C.S. and Leissa, A.W. (1995), "Comprehensive exact solutions for free vibrations of thick annular sectorial plates with simply supported radial edges", *Int. J. Mech. Sci.*, **37**(5), 537-566.
- Mori, T. and Tanaka, K. (1973), "Average stress in matrix and average elastic energy of materials with misfitting inclusions", *Acta Metall.*, **21**(5), 571-574.
- Mukhopadhyay, M. (1979), "A semi-analytic solution for free vibration of annular sector plates", *J. Sound Vib.*, **63**(1), 87-95.
- Mukhopadhyay, M. (1982), "Free vibration of annular sector plates with edges, possessing different degrees

- of rotational restraints”, *J. Sound Vib.*, **80**(2), 275-279.
- Nie, G.J. and Zhong, Z. (2008), “Vibration analysis of functionally graded annular sectorial plates with simply supported radial edges”, *Compos. Struct.*, **84**(2), 167-176.
- Nie, G.J. and Zhong, Z. (2010), “Dynamic analysis of multi-directional functionally graded annular plates”, *Appl. Math. Modell.*, **34**(3), 608-616.
- Pelletier Jacob, L. and Vel Senthil, S. (2006), “An exact solution for the steady state thermo- elastic response of functionally graded orthotropic cylindrical shells”, *Int. J. Solid Struct.*, **43**(5), 1131-1158.
- Ramakris, R. and Kunukkas, V.X. (1973), “Free vibration of annular sector plates”, *J. Sound Vib.*, **30**(1), 127-129.
- Shen, H.S. (2009), “A comparison of buckling and post buckling behavior of FGM plates with piezoelectric fiber reinforced composite actuators”, *Compos. Struct.*, **91**(3), 375-384.
- Shu, C. and Wang C.M. (1999), “Treatment of mixed and non-uniform boundary conditions in GDQ vibration analysis of rectangular plates”, *Eng. Struct.*, **21**(2), 125-134.
- Srinivasan, R.S. and Thiruvengkatachari, V. (1983), “Free vibration of annular sector plates by an integral equation technique”, *J. Sound Vib.*, **89**(3), 425-432.
- Srinivasan, R.S. and Thiruvengkatachari, V. (1986), “Free vibration analysis of laminated annular sector plates”, *J. Sound Vib.*, **109**(1), 89-96.
- Tahouneh, V. and Yas, M.H. (2012), “3-D free vibration analysis of thick functionally graded annular sector plates on Pasternak elastic foundation via 2-D differential quadrature method”, *Acta Mech.*, **223**(9), 1879-1897.
- Tahouneh, V. and Yas, M.H. (2013), “Influence of equivalent continuum model based on the Eshelby-Mori-Tanaka scheme on the vibrational response of elastically supported thick continuously graded carbon nanotube-reinforced annular plates”, *Polym. Compos.*, DOI:10.1002/pc.22818.
- Valery, V., Vasiliev E. and Morozov, V. (2001), *Mechanics and Analysis of Composite Materials*, First Edition, Elsevier Science Ltd.
- Vel, S.S. (2010), “Exact elasticity solution for the vibration of functionally graded anisotropic cylindrical shells”, *Compos. Struct.*, **92**(11), 2712-2727.
- Vel, S.S. and Batra, R.C. (2002), “Exact solution for thermoelastic deformations of functionally graded thick rectangular plates”, *AIAA J.*, **40**(7), 1421-1433.
- Yang, J. and Shen, H.S. (2001), “Dynamic response of initially stressed functionally graded rectangular thin plates”, *Compos. Struct.*, **54**(4), 497-508.
- Yang, J. and Shen, H.S. (2003), “Non-linear analysis of functionally graded plates under transverse and in-plane loads”, *Int. J. Nonlin. Mech.*, **38**(4), 467-482.
- Yas, M.H. and Tahouneh, V. (2012), “3-D free vibration analysis of thick functionally graded annular plates on Pasternak elastic foundation via differential quadrature method (DQM)”, *Acta Mech.*, **223**(1), 43-62.
- Zhou, D., Cheung, Y.K., Lo, S.H. and Au, F.T.K. (2004), “Three-dimensional vibration analysis of rectangular thick plates on Pasternak foundation”, *Int. J. Numer. Method. Eng.*, **59**(10), 1313-1334.
- Zhou, D., Lo, S.H. and Cheung, Y.K. (2009), “3-D vibration analysis of annular sector plates using the Chebyshev-Ritz method”, *J. Sound Vib.*, **320**(1-2), 421-437.
- Zhou, D., Lo, S.H., Au, F.T.K. and Cheung, Y.K. (2006), “Three-dimensional free vibration of thick circular plates on Pasternak foundation”, *J. Sound Vib.*, **292**(3-5), 726-741.